

Void formation in amorphous germanium due to high electronic energy deposition

K. Gärtner,¹ J. Jöhrens,¹ T. Steinbach,^{1,*} C. S. Schnorr,¹ M. C. Ridgway,² and W. Wesch³

¹*Institut für Festkörperphysik, Friedrich-Schiller-Universität Jena, Max-Wien-Platz 1, D-07743 Jena, Germany*

²*Research School of Physics and Engineering, Australian National University, Canberra, Australian Capital Territory 0200, Australia*

³*Institut für Festkörperphysik, Friedrich-Schiller-Universität Jena, Max-Wien-Platz 1, D-07743 Jena, Germany*

(Received 17 March 2011; published 21 June 2011)

The effect of high electronic energy deposition in amorphous germanium has been studied experimentally by Au irradiation with ion energies of up to 185 MeV and different angles of incidence and by molecular dynamics computer simulations. In both cases, the energy deposition leads to void formation accompanied by strong swelling of the amorphous germanium. The simulation results prove that the formation of the voids is mainly based on a shock wave mechanism and the swelling is determined by the competing processes of the formation and growth of voids on the one hand and the shrinking and annihilation of voids on the other hand. In full agreement between experiment and simulation, the amount of the swelling is a linear function of the total energy deposited into electronic processes and there exists a threshold value of the electronic energy loss per ion and depth for swelling. A comparison of the threshold values obtained by the experiment and the simulation suggests that approximately 20% of the energy deposited into electronic processes is converted into atomic motion.

DOI: [10.1103/PhysRevB.83.224106](https://doi.org/10.1103/PhysRevB.83.224106)

PACS number(s): 61.80.Jh, 61.43.Bn, 81.05.Gc, 81.05.Rm

I. INTRODUCTION

Ion irradiation induced morphological changes in amorphous germanium (a-Ge) were first reported during low energy heavy ion irradiation (several hundred keV).¹⁻⁸ In this energy range the ions are stopped mainly by elastic scattering with the target atoms (nuclear energy loss per ion and depth ε_n). The drastic morphological changes are caused by the formation of voids close to the surface and the resulting transformation of the amorphous material into a spongelike structure. This effect consequently leads to a strong swelling of the irradiated part of the sample.

Swift heavy ion (SHI) irradiation of crystalline germanium (c-Ge) also exhibited a swelling of the irradiated material.⁹ In this energy range the ions mainly deposit energy via inelastic scattering with the target atoms (electronic energy loss per ion and depth ε_e) over the first few micrometers of the ion trajectory while nuclear energy deposition dominates near the projected range of the ions. In contrast to the low energy irradiation mentioned above, the authors showed that in this case the origin of the volume expansion was the formation of a *buried* spongelike porous layer whereas the surface of the sample was still crystalline. This buried porous layer was formed at approximately two-thirds of the depth of the nuclear energy deposition maximum suggesting that the formation depends on both ε_e and ε_n .^{9,10}

Recently, we showed that an initially amorphous germanium surface layer (thickness $d = 3.1 \mu\text{m}$) also transforms into a spongelike structure during SHI irradiation.^{10,11} However, in this case ε_n is negligible within the amorphous layer and the structural modification is solely due to the high electronic energy loss per ion and per depth.

The aim of this paper is the investigation of the void formation in a-Ge and the resulting swelling with the help of molecular dynamics computer simulation. We show that the simulation provides unique information about the void formation process and is able to reproduce the experimentally observed dependence of the swelling on the irradiation parameters. In Sec. II the experimental results are briefly

reviewed to allow comparison with the results obtained from simulation. The details of the simulation are summarized in Sec. III while the results are presented and discussed in Sec. IV, followed by a summary and conclusion in Sec. V.

II. EXPERIMENTAL RESULTS

Void formation within the amorphous layer was studied for different electronic energy loss per ion and depth between $\varepsilon_e = 14.0 \dots 38.6 \text{ keV nm}^{-1}$ as estimated by SRIM 2008 calculations¹² by varying the energy and the angle of incidence of the ions [irradiations were performed at the Australian National University (ANU), Canberra]. For all irradiation conditions, a strong elevation of the irradiated a-Ge surface layer with respect to the unirradiated part was observed.¹⁰ The ratio of the corresponding step height Δz and the thickness of the unirradiated amorphous layer d are shown as a function of the ion fluence N_I in Fig. 1. As can be seen, the relative step height $\frac{\Delta z}{d}$ increases with increasing ion fluence for all irradiation parameters used and exhibits a linear dependence on the ion fluence, where the slope increases with increasing ion energy and increasing angle of incidence. This slope $\frac{\Delta z}{N_I d}$ is plotted versus the electronic energy loss per ion and depth ε_e in Fig. 2. It can be seen that in spite of the different ion energies and directions of incidence, the slope is only a function of ε_e , which implies that the swelling is determined solely by the electronic energy loss per ion and per depth. Furthermore, the dependence on ε_e is linear and the extrapolation of the regression line reveals the existence of an electronic energy deposition threshold of about $\varepsilon_{e,\text{th}} = 10.5 \pm 1.0 \text{ keV nm}^{-1}$ above which swelling begins in a-Ge under SHI irradiation at room temperature.¹⁰

Cross section scanning electron microscopy (cs-SEM) of the irradiated samples reveals the reason for the swelling effect as becomes obvious from the example given in Fig. 3. The transformation of the initially homogeneous a-Ge surface layer into a void rich structure is clearly visible. The underlying c-Ge substrate is free of voids showing that void formation takes place solely in the $3.1 \mu\text{m}$ thick amorphous surface layer. The

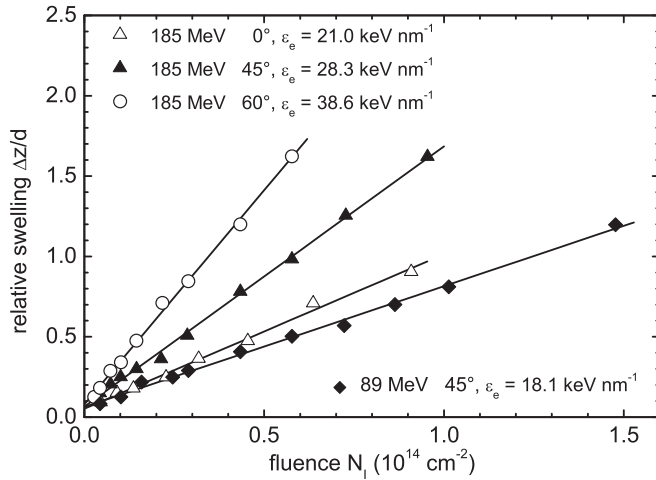


FIG. 1. The relative swelling $\frac{\Delta z}{d}$ of an amorphous Ge layer (swelling Δz divided by the initial thickness of the amorphous Ge layer $d = 3.1 \mu\text{m}$) due to the irradiation with Au ions as a function of the fluence N_I . The irradiation is performed at room temperature with different energies and angles of incidence of the Au ions. The linear fits are given by the lines.

sharp interface is thus preserved despite the irradiation. The voids themselves are randomly distributed, irregularly shaped, and have sizes between 15 and 100 nm. A part of the sample which was masked during the irradiation can be seen in the right section of the SEM image. Here, no voids were generated and the elevation of the irradiated part, Δz , is obvious. Based on these experimental results, one may therefore conclude that voids are formed in a-Ge if a specific threshold value of the energy transferred by electronic processes ($\varepsilon_{e,\text{th}} = 10.5 \pm 1.0 \text{ keV nm}^{-1}$) is exceeded. The resulting swelling depends linearly on the total energy deposited into the amorphous layer and is thus a linear function of both electronic energy loss per ion and depth ε_e and ion fluence N_I .¹⁰

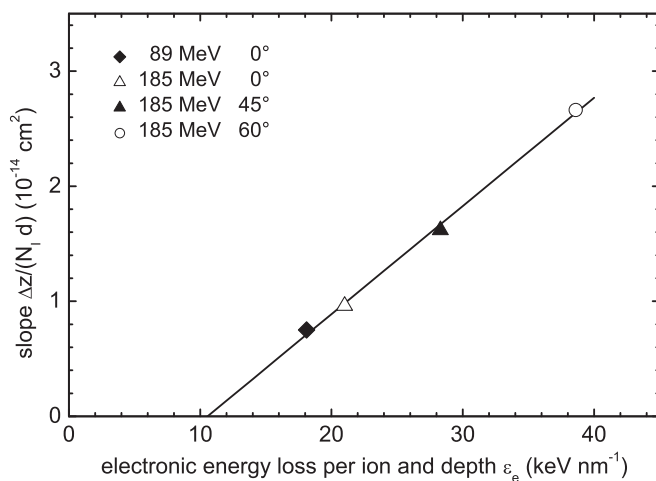


FIG. 2. The slopes $\frac{\Delta z}{N_I d}$ of the linear fits in Fig. 1 as a function of the electronic energy deposition per ion and depth ε_e .

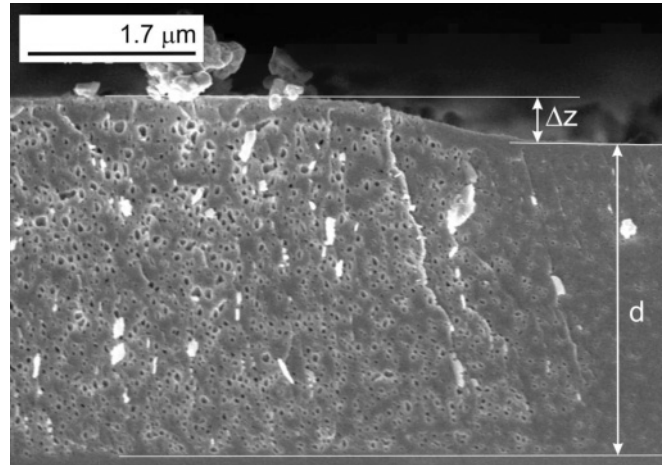


FIG. 3. cs-SEM image showing the transformation of the initially homogeneous a-Ge layer into a void rich a-Ge layer with swelling Δz caused by the irradiation with 185 MeV Au ions under an angle of 45° with a fluence of $7.0 \times 10^{12} \text{ cm}^{-2}$ at room temperature.

III. MOLECULAR DYNAMICS SIMULATION

The molecular dynamics (MD) computer simulations were done with a standard MD code, where the integration of the equations of motion is performed using the velocity form of the Verlet algorithm. The time step is given by the velocity of the fastest atom; however, the maximum value is 0.5 fs. For the interaction between the Ge atoms a potential of the Stillinger-Weber type¹³ splined to a more realistic repulsive pair potential¹⁴ for small interatomic distances was used. The parameters for Ge were taken from Ref. 15. The initial MD cell of the a-Ge consists of 9000 atoms with a size of $85.8 \text{ \AA} \times 85.8 \text{ \AA} \times 26.6 \text{ \AA}$ (mass density 5.147 g cm^{-3}). Note that the size of the MD cell and the mass density change during the simulation. The a-Ge has been prepared by simulating the ion irradiation of c-Ge using a procedure similar to that given in Ref. 16. Figure 4 shows the radial distribution function of the simulated a-Ge in comparison with the corresponding experimental results¹⁷ obtained by X-ray diffraction. The excellent agreement between simulation and experiment proves the accuracy of both the potential and the cell preparation with respect to the description of the a-Ge. To study the influence of the size of the MD cell, a few simulations were performed with MD cells consisting of 18 000 atoms (initial size of $85.8 \text{ \AA} \times 85.8 \text{ \AA} \times 57.2 \text{ \AA}$) and 27 000 atoms (initial size of $85.8 \text{ \AA} \times 85.8 \text{ \AA} \times 85.8 \text{ \AA}$). However, it must be emphasized that even for the largest MD cell, the validity of the simulation is limited to the formation of small voids. According to the experimental results this corresponds to the initial stage of the void formation (the growth of voids up to about 100 nm as found experimentally would require MD cells more than 10 times larger and computing times more than 10^5 times larger for reaching the same fluence).

The swift heavy ion irradiation is simulated in the following simplified way. A given ion penetrates the MD cell in the z direction at zero angle of incidence and at a position (x_0, y_0) . All atoms in a cylinder centered at (x_0, y_0) and with a radius r_{dep} receive additional kinetic energy. This cylinder is called the deposition cylinder in the following. The total amount of

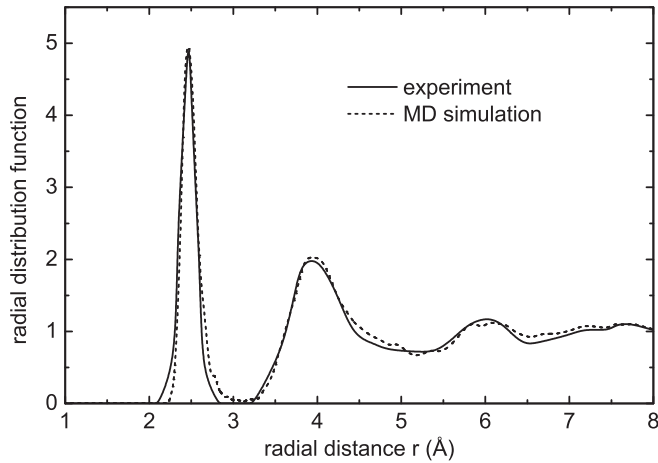


FIG. 4. The radial distribution function of a-Ge at room temperature calculated by MD computer simulation using the small MD cell of 9000 atoms (dashed line) and the corresponding experimental data of Temkin *et al.* (Ref. 17) obtained by X-ray diffraction (solid line).

kinetic energy given to the atoms in the deposition cylinder is $\Delta E_{\text{kin}} = \varepsilon d$ with $\varepsilon = g\varepsilon_e$, where ε is the part of the electronic energy loss per ion and depth ε_e which is converted into atomic motion and d is the z extension of the initial MD cell. The ratio g (< 1) is unknown and used here as a free parameter (in the literature values on the order of 0.1 are mentioned¹⁸ for $A_{\text{III}}B_{\text{V}}$ compounds). The additional kinetic energy ΔE_{kin} is equally divided among all atoms in the deposition cylinder over a time interval of $t_{\text{dep}} = 1$ ps where the directions of the transferred momentums are chosen at random. The time interval t_{dep} used is a characteristic time for the transition of the energy from the electronic system to the motion of atoms¹⁹ and with respect to these investigations it has been shown not to be a critical parameter. As the radius r_{dep} of the deposition cylinder the value $r_{\text{dep}} = 20$ Å was used which is supported by Waligorsky *et al.*²⁰ In one case r_{dep} is varied in order to estimate the influence of the choice of the value of r_{dep} on the results. In contrast to the deposition time, the radius of the deposition cylinder does have a certain influence on the results.

After the energy deposition of a given ion, the evolution of the system is simulated using periodic boundary conditions for all three directions. During the simulation the pressure is kept to zero by allowing the MD cell to expand only in the z direction (swelling) which corresponds to the situation in the experiment. The heat introduced by the energy deposition is extracted by velocity scaling of all atoms outside a cylinder with a radius r_{scal} coaxial to the deposition cylinder (r_{scal} about 0.3 times the x - y diagonal of the MD cell has been shown to be a good choice). After 100 ps the temperature in the MD cell has again reached the initial temperature (room temperature in most cases) and the next ion penetrates the MD cell at a different position (x_0, y_0) which is chosen randomly. That is, the full SHI irradiation is simulated by a series of ions (energy deposition processes) penetrating the MD cell in time intervals of 100 ps at different positions (x_0, y_0) which are equally distributed within the x - y extension of the MD cell. The quantities of interest are the relative swelling $\frac{\Delta z}{d}$ (change of the z extension of the MD cell Δz divided by the

initial z extension of the MD cell d which is equal to the initial thickness of the amorphous layer) and the change of the structure (formation of voids).

IV. RESULTS AND DISCUSSION

Most of the simulations were performed for room temperature $T = 293$ K using the small MD cell consisting of 9000 Ge atoms and the radius of the deposition cylinder $r_{\text{dep}} = 20$ Å. In this case the energy loss per ion and depth ε has been widely varied between 1.7 keV nm⁻¹ and 3.4 keV nm⁻¹. The corresponding results range from approximately zero effect up to 150% swelling caused by the formation of voids. In Sec. IV A, the results obtained for $\varepsilon = 2.6$ keV nm⁻¹ are presented and discussed as a typical example for the formation of voids. First, the effect resulting from one ion (one energy deposition) is investigated and second, a sequence of ions (ion beam) is considered. In Sec. IV B, the swelling as a function of the fluence is considered for comparison with experimental data, where the energy loss per ion and depth ε , the radius of the deposition cylinder r_{dep} , and the temperature T are varied.

A. Void formation

The results for the impact of one ion for fixed parameters ($\varepsilon = 2.6$ keV nm⁻¹, $T = 293$ K, $r_{\text{dep}} = 20$ Å; impact position is the center of the x - y plane of the MD cell) are presented in Figs. 5–9. The relative swelling $\frac{\Delta z}{d}$ and the average temperature and pressure in the MD cell as functions of the time are depicted in Fig. 5. As can be seen, the relative swelling increases rapidly up to a maximum value of about 18% at $t = 2.9$ ps followed by a decrease until it reaches a constant value of 7% already at about $t = 50$ ps. The temperature behaves similarly. It reaches the initial value (293 K) well before $t = 100$ ps. The pressure oscillates with a strong decrease of its amplitude (constant pressure regime) and it reaches zero again after about 20 ps. All the data in Fig. 5 indicate that the essential

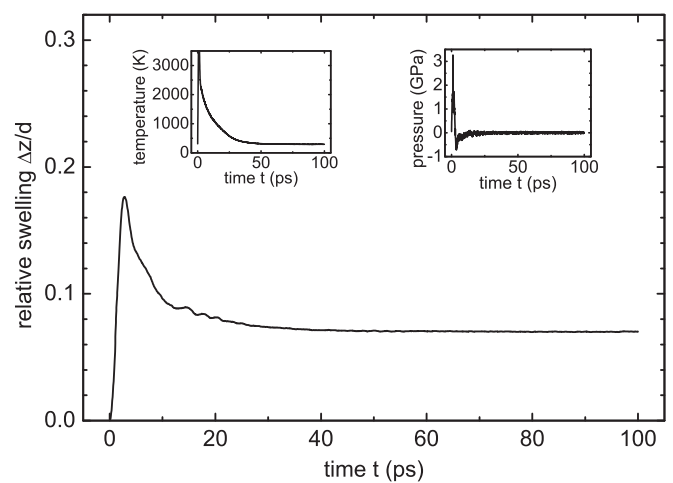


FIG. 5. The relative swelling $\frac{\Delta z}{d}$ (change of the z extension of the MD cell divided by the initial z extension of the MD cell $d = 26.6$ Å) and the average temperature and pressure in the MD cell as functions of the time for one ion impinging the center of the x - y plane of the MD cell at the time $t = 0$. The energy deposition starts at $t = 0$ and is finished at $t = 1$ ps.

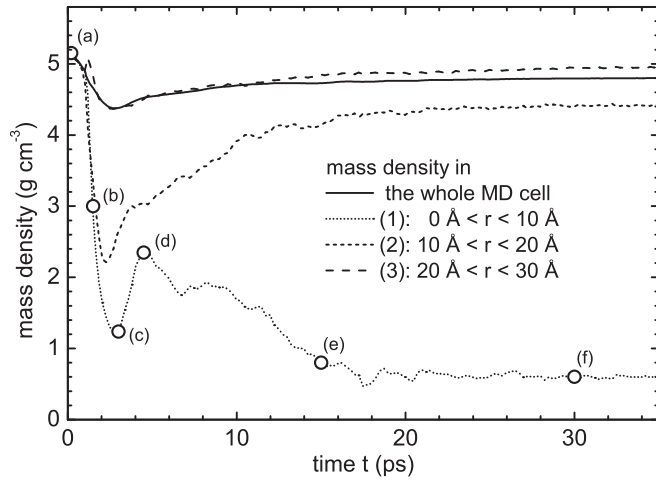


FIG. 6. The average mass densities of all atoms in the MD cell and of three different cylinder shells as functions of the time t for one ion impinging the MD cell at $t = 0$ ($\epsilon = 2.6 \text{ keV nm}^{-1}$, $T = 293 \text{ K}$, $r_{\text{dep}} = 20 \text{ \AA}$). The cylinder shells are coaxial to the deposition cylinder and r is the radial distance from the axis of the deposition cylinder, the position of which is given by the impact position of the ion [here the center of the x - y plane, see also Fig. 7(a)]. For some times labeled by (a) to (f), the configurations of the atoms in the MD cell are visualized in Fig. 7.

processes responsible for the swelling take place mainly within about 30 ps. Therefore, the evolution of the a-Ge system in this time interval is investigated in more detail. Instead of the relative swelling, the corresponding average mass density of all atoms in the MD cell is depicted in Fig. 6 (solid line). In order to get some information about the distribution of the atoms, the average mass densities of all atoms within three different cylinder shells (coaxial to the deposition cylinder) as functions of the time are added in Fig. 6. The strongest change takes place in the cylinder (1) with radius 10 \AA which is much smaller than the deposition cylinder ($r_{\text{dep}} = 20 \text{ \AA}$). For some characteristic times labeled by (a) to (f), the top views (onto the x - y plane) of the corresponding configurations of the atoms in the MD cell are presented in Fig. 7. The snapshot Fig. 7(a) shows the initial MD cell, where the atoms within the deposition cylinder are highlighted. At about 1.5 ps, the mass densities in cylinder (1) and in cylinder shell (2) as well as are reduced to about 60% [Fig. 6(b)], but the mass density in the cylinder shell (3) does not change remarkably. This means that the reduction of the density is approximately restricted to the volume of the deposition cylinder which can also be seen in Fig. 7(b). At about 3 ps, the density in the cylinder (1) reaches a local minimum and is much lower than that in cylinder shell (2) (Fig. 6). As can be seen in Fig. 7(c), this corresponds to a latent void (radius of about 4 \AA) and a reduced density around it. This void disappears about 1.5 ps later and leaves a region of reduced density [Figs. 6(d) and 7(d)]. At 15 ps a void is formed again, however, still with a diffuse interface [Fig. 7(e)]. With proceeding time the interface becomes more and more sharp resulting in a stable void (proved for times up to 1 ns) with a radius of about 9 \AA [Fig. 7(f)]. As can be seen in Fig. 6, the density in cylinder shell (2) recovers to 86% of the initial value. The time dependence of the mass density outside the deposition cylinder [cylinder

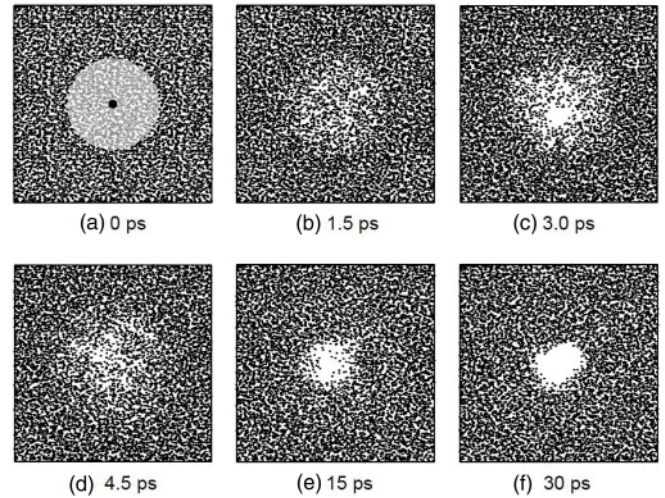


FIG. 7. The top views (onto the x - y plane) of the configurations of the atoms (small full dots) in the MD cell at the different times labeled by (a) to (f) in Fig. 6 (note that only the z extension of the MD cell changes with time; the x - y extension $85.8 \text{ \AA} \times 85.8 \text{ \AA}$ remains constant). In panel (a), the impact position of the ion is marked by the large full dot and all the atoms within the deposition cylinder (radius $r_{\text{dep}} = 20 \text{ \AA}$) are highlighted.

shell (3)] is about the same as that of the whole MD cell. The essential difference is the interesting peak at about 1.3 ps. This gives rise to a more detailed investigation of the mass density outside the deposition cylinder in this time interval. The results are presented in Fig. 8. As can be seen, there is a rapid change of the mass densities in the three different cylinder shells outside the deposition cylinder which is typical for a shock wave. The time at which the increase of the density for a given cylinder shell is about half of the corresponding maximum increase (full dots in Fig. 8) is used as the time of

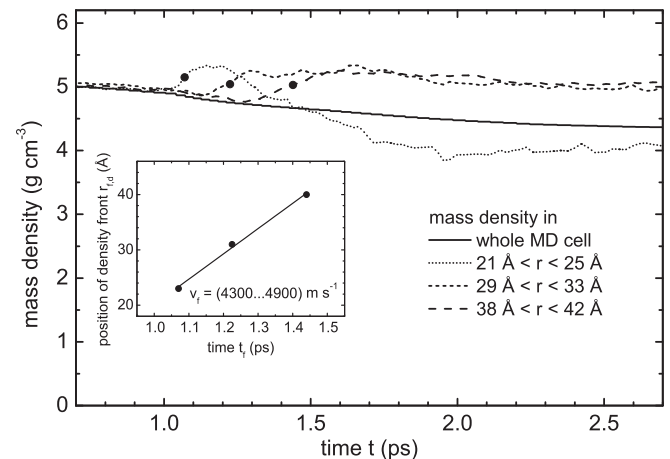


FIG. 8. The average mass density of all atoms in the MD cell and in three different cylinder shells outside the deposition cylinder as functions of the time t for one ion impinging the MD cell at $t = 0$ (same conditions as in Fig. 6). The times t_f when the mass density front reaches the different cylinder shells (with average positions $r_{f,d} = 23 \text{ \AA}$, 31 \AA , and 40 \AA , respectively) are marked by the full dots. In the inset, the positions $r_{f,d}$ are plotted over the time t_f . The solid line is the corresponding linear fit.

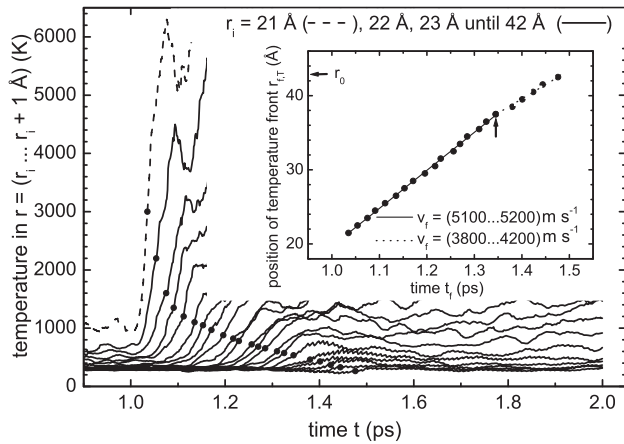


FIG. 9. The average temperatures of all atoms in 22 different cylinder shells ($21 \text{ \AA} \leq r < 22 \text{ \AA}$, $22 \text{ \AA} \leq r < 23 \text{ \AA}$ until $42 \text{ \AA} \leq r < 43 \text{ \AA}$) outside the deposition cylinder as functions of the time t for one ion impinging the MD cell at $t = 0$ (same conditions as in Fig. 6). The times t_f when the temperature front reaches the different cylinder shells (with average positions $r_{f,T} = 21.5 \text{ \AA}$ up to 42.5 \AA , respectively) are marked by the full dots. In the inset the positions $r_{f,T}$ are plotted over the time t_f . The solid line and the dotted line are the linear fits in the two time intervals separated by $t_f = 1.35 \text{ ps}$ (marked by the arrow). The radius $r_0 = 42.9 \text{ \AA}$ is half of the x extension of the MD cell.

arrival of the density wave front t_f at the position $r_{f,d}$ which is the average value of r in this cylinder shell. The inset of Fig. 8 shows the position of the front $r_{f,d}$ as a function of the time t_f . There is an approximately linear dependence providing a velocity of the density wave front $v_f = (4600 \pm 300) \text{ m s}^{-1}$. This velocity seems to exceed the sound velocity in a-Ge which is $(4000 \pm 50) \text{ m s}^{-1}$ according to the experimental results of Cox-Smith *et al.*²¹ A more precise determination of the wave front velocity is obtained by studying the evolution of the temperature wave front. The results are shown in Fig. 9. Because the statistical fluctuations are lower than those for the density, the temperature can be determined in cylinder shells with much smaller thicknesses (here 1 \AA instead of 4 \AA for the density) which provides a larger number of values for the position of the front. Furthermore, the time of arrival of the temperature wave front t_f can be determined more precisely than that of the density wave front because the relative change of the temperature at the front is much larger ($> 150\%$ up to 1.35 ps and $> 35\%$ above) than the relative change of the density ($7\% \dots 12\%$) (compare Figs. 8 and 9). The resulting times of arrival of the temperature wave front t_f and the corresponding positions of the wave front $r_{f,T}$ (both determined as in Fig. 8) are depicted in the inset of Fig. 9. As can be seen, the position of the wave front $r_{f,T}$ is a linear function of the time t_f up to about $t_f = 1.35 \text{ ps}$ (marked by the vertical arrow) providing a wave front velocity $v_f = (5150 \pm 50) \text{ m s}^{-1}$. For $t_f > 1.35 \text{ ps}$ there is again a linear dependence of $r_{f,T}$ on t_f , however, with a smaller slope corresponding to a wave front velocity $v_f = (4000 \pm 200) \text{ m s}^{-1}$. At about 1.5 ps the wave front reaches the edge of the MD cell ($r_{f,T} = r_0$). As already mentioned above, the experimentally determined sound velocity in a-Ge is $(4000 \pm 50) \text{ m s}^{-1}$.²¹ This means that the wave front definitely

moves with supersonic velocity at first and from about 1.35 ps it propagates as an ordinary sound wave with exactly the measured sound velocity which are both characteristic features of a shock wave (see, e.g., Ref. 22). These results prove that the void formation in a-Ge is mainly based on a shock wave mechanism. In addition, they provide another argument for the applicability of the interaction potential between the Ge atoms used here (Stillinger-Weber type) and the quality of the prepared a-Ge because the sound velocity of a-Ge is also obtained correctly.

Up to now, the formation of a void caused by the impact of one ion at the center of the x - y plane of the MD cell has been investigated. In the following a sequence of ions (ion beam) is considered. The different impact positions of the ions (x_0, y_0) are chosen at random according to a uniform distribution within the x - y extension of the MD cell. Because all the physical quantities of interest here reach equilibrium constant values in a time less than 100 ps after the impact of an ion (see Fig. 5), the succeeding ions are started in time intervals of 100 ps . The resulting relative swelling $\frac{\Delta z}{d}$ as a function of the time is depicted in Fig. 10. The empty dots represent the values of $\frac{\Delta z}{d}$ reached as a result of the preceding ion before the next ion starts. The additional small full dots mark the times for which the corresponding configurations of the atoms in the MD cell are shown in Fig. 11. The void formed by the impact of ion 1 and the resulting relative swelling have already been described above. The increase of the relative swelling $\frac{\Delta z}{d}$ with increasing number of ions (Fig. 10) is determined by the formation, growth, shrinking, and annihilation of voids, where in almost all cases the formation and growth are the more effective processes. For some typical examples this is demonstrated in Fig. 11. The change of the structure caused by the impact of a given ion is visualized by two snapshots. The left snapshot

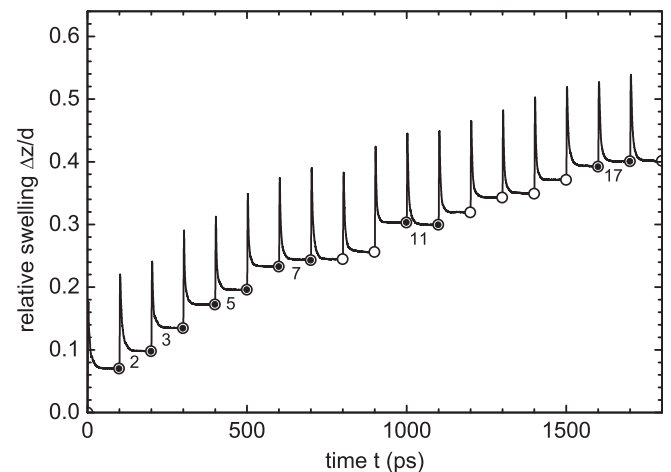


FIG. 10. The relative swelling $\frac{\Delta z}{d}$ as a function of the time t for irradiation with a sequence of ions started in time intervals of 100 ps (solid line). The empty dots represent the asymptotic values of $\frac{\Delta z}{d}$ reached as a result of the preceding ion before the next ion starts (that means before the sharp peak). The changes of the configurations of the atoms in the MD cell caused by ions 2, 3, 5, 7, 11, and 17 (the corresponding time intervals are labeled by the numbers of the ions and the limits of these intervals are marked by the small full dots) are visualized in Fig. 11. The conditions are given by $\varepsilon = 2.6 \text{ keV nm}^{-1}$, $T = 293 \text{ K}$, and $r_{\text{dep}} = 20 \text{ \AA}$.

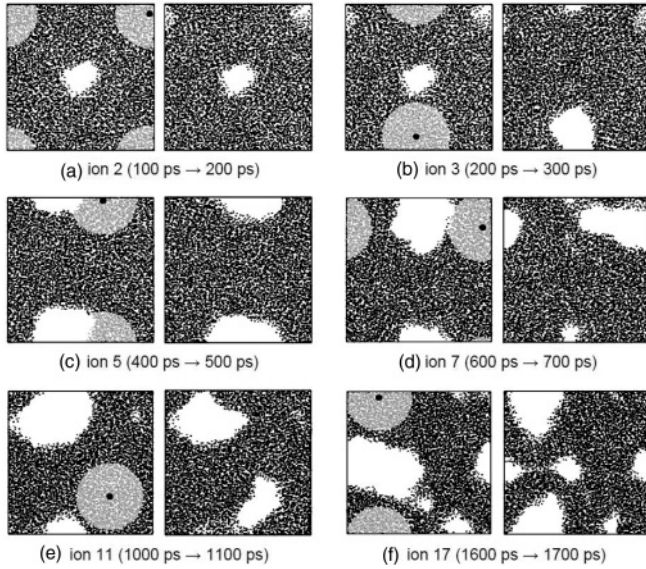


FIG. 11. The top views (onto the x - y plane) of the configurations of the atoms (small dots) in the MD cell before starting a given ion and 100 ps later, that is, before starting the next ion. The time intervals belonging to the ions considered are also marked in Fig. 10 by the numbers of these ions. As in Fig. 7, the impact positions of the ions are marked by the large full dots and all atoms within the deposition cylinders (radius $r_{\text{dep}} = 20 \text{ \AA}$) are highlighted. Note that the x - y extension of the MD cell ($85.8 \text{ \AA} \times 85.8 \text{ \AA}$) does not change and periodic boundary conditions in the x and y directions are used.

shows the situation when this ion starts, where the position of the ion impact is marked by the full black dot and the atoms within the deposition cylinder (excited atoms) are highlighted. The right snapshot shows the resulting structure reached 100 ps later. This time interval is also marked in Fig. 10 by the number of the corresponding ion. As can be seen, ion 2 generates a small void around its impact position and the initially existing void remains [Fig. 11(a)]. Ion 3 is responsible for the formation of a new void and the annihilation of the existing void. The small void caused by ion 2 remains [Fig. 11(b)]. As the result of the impact of ion 5 [Fig. 11(c)], the existing void grows. Caused by the impact of ion 7 [Fig. 11(d)], a new void is generated and the initially existing void shrinks remarkably. Therefore, the corresponding increase of $\frac{\Delta z}{d}$ is smaller than in the previous cases (see Fig. 10). Ion 11 [Fig. 11(e)] generates a new void; however, the initially existing large void shrinks so much that in this case the relative swelling even decreases (see Fig. 10). The final result after irradiation with 17 ions is a spongelike structure shown in Fig. 11(f) and a total swelling of about 40% (Fig. 10). Considering all the snapshots in Fig. 11, a relation between the results of the ion impact and the impact position relative to already existing voids can be found. If there are no voids within the deposition cylinder, only a new void is generated [Fig. 7 and Fig. 11(a)] or a new void is generated and the previous void shrinks [Figs 11(d) and 11(e)] or even disappears [Fig. 11(b)]. If a significant part of an existing void intersects the deposition cylinder, this void grows [Fig. 11(c)] and mostly nothing else happens. In order to study the stability of these structures a very strongly swelled a-Ge cell with $\frac{\Delta z}{d} = 0.665$ (not seen in Fig. 10) has been annealed at 293 K

and at 1000 K up to 2 ns (not shown). No visible effect has been found at 293 K. At the annealing temperature of 1000 K, $\frac{\Delta z}{d}$ decreases by 16% up to 1 ns caused by a sharpening of the internal surfaces but there is no further change up to 2 ns. This means the structures obtained after irradiation are thermally stable.

B. Fluence dependence of the swelling

For comparison with the experimental results (Figs. 1 and 2), the relative swelling as a function of the time (as, e.g., shown in Fig. 10) is converted into a dependence on the fluence N_I by $N_I = t/(100 \text{ ps } A_{\text{MD}})$, where $A_{\text{MD}} = 7362 \text{ \AA}^2$ is the x - y area of the MD cell which remains constant. First, the results obtained for different energy losses per ion and depth ε are presented, second the influence of the size of the MD cell and the choice of the radius of the deposition cylinder r_{dep} are investigated, and third, a preliminary result for different irradiation temperatures is given.

Figure 12 shows the relative swelling $\frac{\Delta z}{d}$ as a function of the fluence N_I for different energy losses per ion and depth ε where the values of the temperature ($T = 293 \text{ K}$) and the radius of the deposition cylinder ($r_{\text{dep}} = 20 \text{ \AA}$) are the same as used in Sec. IV A. As can be seen, for all values $\varepsilon \geq 2.6 \text{ keV nm}^{-1}$ the relative swelling increases linearly with increasing fluence over nearly the whole fluence range. Only for very small fluences up to about $0.02 \dots 0.05 \times 10^{14} \text{ cm}^{-2}$ the increase is stronger. The linear dependence of the relative swelling on the fluence, and also the stronger increase for the very small fluences, is in good qualitative agreement with the experimental results (see Fig. 1). For $\varepsilon \leq 2.3 \text{ keV nm}^{-1}$ there is only a small initial swelling that does not further increase with increasing fluence. The small constant swelling is obviously caused by point defects or very small instable voids in the a-Ge which are of no further interest here. The results in Fig. 12 indicate the existence of a threshold value ε_{th} for swelling analogously to the threshold value of $\varepsilon_{e,\text{th}}$

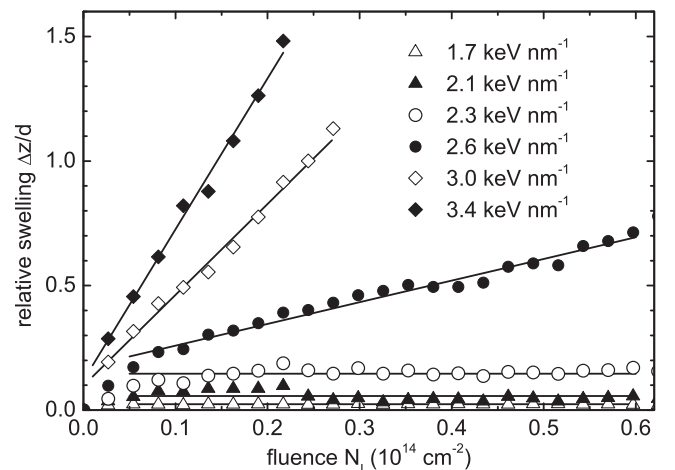


FIG. 12. The relative swelling $\frac{\Delta z}{d}$ as a function of the fluence N_I for different values of the energy loss per ion and depth ε ($T = 293 \text{ K}$, $r_{\text{dep}} = 20 \text{ \AA}$). The symbols represent the asymptotic values of $\frac{\Delta z}{d}$ as defined in Fig. 10 (in order to reduce the number of symbols only the values of ions with even numbers are depicted). The solid lines are the corresponding linear fits.

found experimentally (Fig. 2). The threshold value ε_{th} is determined in the same way as that of $\varepsilon_{e,\text{th}}$ in Fig. 2. For this purpose, the slopes $\frac{\Delta z}{N_I d}$ of the linear fits in Fig. 12 are calculated and depicted in Fig. 13 (full dots). As can be seen, in agreement with the behavior of the experimental data (Fig. 2) the slopes show a linear dependence on ε or ε_e (g is assumed to be constant) providing a threshold value $\varepsilon_{\text{th}} = 2.46 \text{ keV nm}^{-1}$.

To study the influence of the size of the MD cell on the threshold value, a few simulations using two MD cells with larger z extensions (18 000 atoms, initial size of $85.8 \text{ \AA} \times 85.8 \text{ \AA} \times 57.2 \text{ \AA}$, and 27 000 atoms, initial size of $85.8 \text{ \AA} \times 85.8 \text{ \AA} \times 85.8 \text{ \AA}$) were performed. The results are added in Fig. 13. The dependence of the slopes $\frac{\Delta z}{N_I d}$ on ε is similar to that obtained using the small MD cell; there is only a shift to lower ε . For the two larger MD cells the shifts are about equal indicating a convergence of the threshold value of ε with respect to the extension of the MD cell in the z direction which is $\varepsilon_{\text{th}} = 2.2 \text{ keV nm}^{-1}$. From this value and the experimentally determined value $\varepsilon_{e,\text{th}} = 10.5 \text{ keV nm}^{-1}$ follows $g = 0.21$ for the relative part of the electronic energy loss per ion and depth ε_e which is converted into atomic motion. The value thus obtained for g is of a similar order as the values of around 0.1 mentioned in the literature for $A_{\text{III}}B_{\text{V}}$ compounds.¹⁸

To estimate the influence of the choice of the radius of the deposition cylinder, the simulations using the smaller MD cell (9000 atoms) have been repeated for $r_{\text{dep}} = 15 \text{ \AA}$ and $r_{\text{dep}} = 25 \text{ \AA}$ (the upper value of r_{dep} is limited by the size of the MD cell). They provide the threshold values $\varepsilon_{\text{th}} = 2.30 \text{ keV nm}^{-1}$ and $\varepsilon_{\text{th}} = 2.62 \text{ keV nm}^{-1}$ for the energy loss per ion and depth, respectively. This means that the threshold value ε_{th} shows a linear dependence on the radius of the deposition cylinder (for $r_{\text{dep}} = 20 \text{ \AA}$ the threshold value is $\varepsilon_{\text{th}} = 2.46 \text{ keV nm}^{-1}$ as mentioned above) within the range of r_{dep} investigated here. These results show that the influence of the choice of the radius of the deposition cylinder must be taken into account but it is not too strong. A variation of r_{dep} by $\pm 25\%$ provides only a variation of ε_{th} by $\pm 6.5\%$.

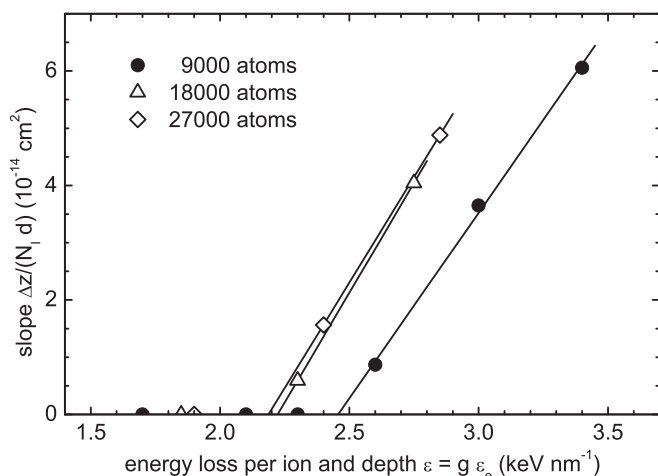


FIG. 13. The slopes $\frac{\Delta z}{N_I d}$ of the linear fits in Fig. 12 as a function of the energy loss per ion and depth ε (full dots). The corresponding results using the larger MD cells (18 000 atoms and 27 000 atoms) are added ($T = 293 \text{ K}$, $r_{\text{dep}} = 20 \text{ \AA}$).

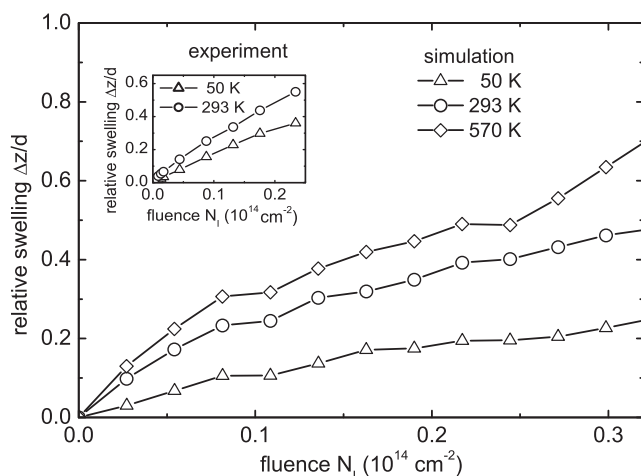


FIG. 14. The relative swelling $\frac{\Delta z}{d}$ as a function of the fluence N_I for $\varepsilon = 2.6 \text{ keV nm}^{-1}$, $r_{\text{dep}} = 20 \text{ \AA}$, and different values of the irradiation temperature. For comparison, preliminary experimental results for two temperatures are shown in the inset. They have been obtained by irradiation of a 3.1 \mu m thick a-Ge layer with 940 MeV Au ions at zero angle of incidence at GSI, Germany.

With respect to the dependence of the swelling on the irradiation temperature, a few simulation results for $\varepsilon = 2.6 \text{ keV nm}^{-1}$ are presented in Fig. 14. As can be seen, the relative swelling increases remarkably with increasing temperature. To check this tendency, preliminary experiments were performed at low temperature (50 K) and at room temperature. They have been obtained by irradiating a 3.1 \mu m thick a-Ge layer with 940 MeV Au ions at 0° at the Gesellschaft für Schwerionenforschung (GSI), Germany. The a-Ge layer was prepared like those irradiated at the ANU (Figs 1–3). The experimental results are added in the inset in Fig. 14. As can be seen, the tendency of the temperature dependence of the relative swelling predicted by the simulation is confirmed by the experimental results and even the strength of this dependence is comparable to that found experimentally [the average ratios $\frac{\Delta z}{d}(50 \text{ K})/\frac{\Delta z}{d}(293 \text{ K})$ of the simulated and experimental results for $N_I > 0.1 \times 10^{14} \text{ cm}^{-2}$ are about 0.5 and 0.6, respectively]. This means that the temperature dependence of the relative swelling is obviously reasonably described by the simulation. However, for a deeper insight more experimental and theoretical investigations are necessary.

V. SUMMARY AND CONCLUSION

The formation of voids in a-Ge due to high electronic energy deposition by swift heavy ions, resulting in a swelling of the a-Ge, is investigated experimentally and with the help of molecular dynamics (MD) computer simulations. The simulation results are shown to be able to give information about the processes of the formation and evolution of the voids, the existence of which has been proven experimentally by cs-SEM. The investigation of the evolution of local densities and temperatures definitely show that acoustic shock waves are generated by the high energy deposition. For a typical case

of energy deposition, the shock wave propagates for about 0.35 ps after the energy deposition with a supersonic velocity $v_f = (5150 \pm 50) \text{ m s}^{-1}$ [the measured sound velocity in a-Ge is $(4000 \pm 50) \text{ m s}^{-1}$; Ref. 21]. Then it decays and continues as an ordinary sound wave with a velocity $v_f = (4000 \pm 200) \text{ m s}^{-1}$, which agrees very well with the measured sound velocity. The fact that shock waves are generated under the conditions of high energy deposition agrees fully with the results of Carter,²² Trinkaus,²³ and Kluth *et al.*²⁴ Carter predicted that for high energy deposition due to swift heavy ions, the core of the spike (which can be assumed to be cylindrical) is a source of shock waves.²² This occurs because in this case the free path of an atom between the collisions is on the order of the mean atomic spacing leading to collective collisions. The shock wave concept has been successfully applied to explain, e.g., very high sputtering rates or exfoliation processes (Ref. 22 and references therein) and the anisotropic growth of amorphous solids under swift heavy ion irradiation.²³ Kluth *et al.* investigated the radial density profiles for tracks in amorphous SiO₂ generated by swift heavy ion irradiation.²⁴ The experimental data show a core of reduced density surrounded by a shell of higher density. They argue that a shock wave is emitted caused by a sudden thermal expansion in the track center. The experimental results are well described by MD computer simulations.²⁴ Our simulations show that the shock wave mechanism is also the main process of the formation of voids which can be understood as an extreme case of the reduction of the density found by Kluth *et al.*²⁴ Within the time range of ns the voids have been proven to be stable even at a temperature of 1000 K.

The swelling of the a-Ge due to the irradiation with swift heavy ions has been shown to be determined by the competing processes of the formation and growth of voids on the one

hand and the shrinking and annihilation of voids on the other hand. Obviously, all these processes are mainly based on the shock wave mechanism. The fact that the swelling of the a-Ge obtained by the simulation depends linearly on the fluence agrees fully with the experimental results. Also in agreement with the experimental results, the simulations provide the existence of a threshold of the energy loss per ion and depth for swelling. The existence of this threshold is independent of the conditions of the simulation considered here; only its absolute value ε_{th} is influenced by the size of the MD cell and the value of the deposition radius r_{dep} . While the value of ε_{th} converges with respect to the extension of the MD cell in the z direction, it depends linearly on the deposition radius r_{dep} . For the large MD cell and $r_{\text{dep}} = 20 \text{ \AA}$ the value $\varepsilon_{\text{th}} = 2.2 \text{ keV nm}^{-1}$ is obtained, where an uncertainty of r_{dep} of 25% provides an uncertainty of ε_{th} of 6.5%. By a comparison with the experimentally determined threshold value $\varepsilon_{e,\text{th}} = 10.5 \text{ keV nm}^{-1}$ for the electronic energy loss per ion and depth, the unknown parameter g ($\varepsilon_{\text{th}} = g\varepsilon_{e,\text{th}}$) can be determined. It provides $g = 0.21$ which is of a similar order as values reported for A_{III}B_V compounds.¹⁸ Preliminary results show that the temperature dependence of the swelling may also be well described by the simulation. However, to fully understand the temperature dependence more detailed investigations are necessary.

ACKNOWLEDGMENTS

The research has been supported by the Bundesministerium für Bildung und Forschung (BMBF, Contract No. 05KK7SJ1) and Deutscher Akademischer Austausch Dienst (DAAD, Contract No. D/07/15034).

*Corresponding author: tobias.steinbach@uni-jena.de

¹I. H. Wilson, *J. Appl. Phys.* **53**, 1698 (1982).

²B. R. Appleton, O. W. Holland, J. Narayan, O. E. Schow, J. S. Williams, K. T. Short, and E. Lawson, *Appl. Phys. Lett.* **41** (8), 711 (1982).

³O. W. Holland, B. R. Appleton, and J. Narayan, *J. Appl. Phys.* **54**, 2295 (1983).

⁴B. R. Appleton, O. W. Holland, D. B. Poker, J. Narayan, and D. Fathy, *Nucl. Instrum. Methods Phys. Res., Sect. B* **7/8**, 639 (1985).

⁵L. M. Wang and R. C. Birtcher, *Philos. Mag. A* **64**, 1209 (1991).

⁶B. Stritzker, R. G. Elliman, and J. Zou, *Nucl. Instrum. Methods Phys. Res., Sect. B* **175-177**, 193 (2001).

⁷T. Janssens, C. Huyghebaert, D. Vanhaeren, G. Winderickx, A. Satta, M. Meuris, and W. Vandervorst, *J. Vac. Sci. Technol. B* **24**, 510 (2006).

⁸J. Yanagisawa, K. Takarabe, K. Ogushi, K. Gamo, and Y. Akasaka, *J. Phys. Condens. Matter* **19**, 445002 (2007).

⁹H. Huber, W. Assmann, R. Grötzschel, H. D. Mieskes, A. Mücklich, H. Nolte, and W. Prusseit, *Mat. Sci. For.* **248/249**, 301 (1997).

¹⁰T. Steinbach, C. S. Schnorr, P. Kluth, R. Giuliani, L. L. Araujo, D. J. Sprouster, M. C. Ridgway, and W. Wesch, *Phys. Rev. B* **83** (5), 054113 (2011).

¹¹W. Wesch, C. S. Schnorr, P. Kluth, Z. S. Hussain, L. L. Araujo, R. Giuliani, D. J. Sprouster, A. P. Byrne, and M. C. Ridgway, *J. Phys. D* **42**, 115402 (2009).

¹²J. F. Ziegler, J. P. Biersack, and U. Littmark, *The Stopping and Range of Ions in Solids* (Oxford, Pergamon, 2003).

¹³F. H. Stillinger and T. A. Weber, *Phys. Rev. B* **31**, 5262 (1985).

¹⁴K. Gärtner and K. Hehl, *Phys. Status Solidi B* **94**, 231 (1979).

¹⁵K. Ding and H. C. Andersen, *Phys. Rev. B* **34**, 6987 (1986).

¹⁶B. Weber, K. Gärtner, and D. M. Stock, *Nucl. Instrum. Methods Phys. Res., Sect. B* **127/128**, 239 (1997).

¹⁷R. J. Temkin, W. Paul, and G. A. N. Connell, *Adv. Phys.* **22**, 581 (1973).

¹⁸G. Szenes, Z. E. Horvath, B. Pecz, F. Paszti, and L. Toth, *Phys. Rev. B* **65**, 045206 (2002).

¹⁹C. Dufour, E. Paumir, and M. Toulemonde, *Radiat. Eff.* **126**, 119 (1993).

²⁰M. P. R. Waligorski, R. N. Hamm, and R. Katz, *Int. J. Rad. Appl. Instr. D* **11**, 309 (1986).

²¹I. Cox-Smith, H. Liang, and R. Dillon, *J. Vac. Sci. Technol. A* **3**, 674 (1985).

²²G. Carter, *Radiat. Eff. Lett.* **43**, 193 (1979).

²³H. Trinkaus, *Nucl. Instrum. Methods Phys. Res., Sect. B* **107**, 155 (1996).

²⁴P. Kluth, C. S. Schnohr, O. H. Pakarinen, F. Djurabekova, D. J. Sprouster, R. Giulian, M. C. Ridgway, A. P. Byrne, C. Trautmann, D. J. Cookson, K. Nordlund, and M. Toulemonde, *Phys. Rev. Lett. B* **101**, 175503 (2008).